ISSN: 2088-8708, DOI: 10.11591/ijece.v15i6.pp5144-5161

# Optimized passive and active shielding of magnetic induction generated by ultra-high-voltage overhead power lines

#### Salah-Eddine Houicher, Rabah Djekidel, Sid Ahmed Bessedik

Department of Electrical Engineering, Faculty of Technology, LACoSERE laboratory, Ammar Telidji University of Laghouat, Laghouat, Algeria

### **Article Info**

#### Article history:

Received Aug 8, 2024 Revised Aug 30, 2025 Accepted Sep 15, 2025

#### Keywords:

Compensation loop Grey wolf optimizer Magnetic induction Optimization Overhead transmission lines Ultra-high-voltage

# **ABSTRACT**

This paper presents computational modeling to assess and limit the magnetic induction levels emitted by an extra-high-voltage (EHV) overhead transmission line of 750 kV using the fundamental principle of Biot-Savart law in magnetostatics. An optimization technique based on the grey wolf optimizer (GWO) algorithm is employed to determine the appropriate location of the passive and active loop conductors, and the associated parameters to shielding to achieve better compensation of magnetic induction in an interest zone. The resulting magnetic induction of the ultra high voltage (UHV) overhead power line exhibits a crest value of 27.78 μT at the middle of the right-of-way, which can be considered unacceptable by strict protection standards. Generally, the magnetic compensation loops optimally located under the phase conductors of the power transmission system reduce the magnetic induction levels along the transmission line corridor. The passive loop attenuates the maximum magnetic induction by a rate of 29.7%. Therefore, the performance of the active loop is better; it provides a greater reduction with a rate reaching 53.24%. The simulation results were tested with those derived by the elliptical polarization process. An excellent concordance was found, which made it possible to ensure the adopted method.

This is an open access article under the <u>CC BY-SA</u> license.



5144

# Corresponding Author:

Rabah Djekidel

Department of Electrical Engineering, Faculty of Technology, Université Amar Telidji

37G Route de Ghardaia - Laghouat, 03000, Algeria

Email: r.djekidel@lagh-univ.dz

#### 1. INTRODUCTION

Electricity is considered a key factor in improving and facilitating the quality of humanity's daily life and stimulating necessary economic development. In effect, the expanding human population and the rapid development of industrialization ipso facto lead to an increased demand for electrical energy. To meet such demand, it becomes necessary to install electricity transmission power lines with a higher voltage level and an elevated initial power rating [1], [2].

In recent decades, the electric and magnetic fields radiated by the overhead transmission lines have increasingly posed concerns about their adverse impacts on population health and environmental quality. Indeed, the higher the transmission line voltage, the more severe the possible effects. The possible short-term and long-term human health consequences of these electromagnetic fields have been the subject of extensive study and intense research over the past 40 years. The short-term biological actions of AC induced electrical current on the human organism are well known. These are reversible effects of simulating nerve and heart cells [3]–[12], [13].

On the other hand, the fears of international society which are expressed mainly concern the possible long-term effects that low and prolonged exposure could have, which can cause major health risks and numerous diseases. It should be noted, however, that this scientific evidence neither categorically supports nor denies these claims at the same time. The International Commission on Non-Ionizing Radiation Protection (ICNIRP) is an international organization legally reaccredited by the World Health Organization (WHO) responsible for protecting people and the environment and providing guidance and advice on risks for health associated with exposure to non-ionizing radiation. In addition, the work and publications of this scientific commission are considered the most reputable, quality and reliable throughout the world. Based on the results and recommendations reported by laboratory research studies and in-depth scientific investigations and in accordance with the precautionary principle, this commission imposed recommendations specifying basic thresholds and safety limits aimed at protecting human health risks linked to exposure to extremely low frequency electric and magnetic fields (ELF-EMF) [14]-[18]. The exposure limits imposed by this commission are estimated over 24 hours, for the general public 5 kV/m for the electric field and 200 µT for the magnetic field, for professional exposure, they are respectively 10 kV/m and 1 mT [18]. Several states over the world have relied the exposure limit values proposed by ICNIRP as national standards, while other countries have taken more severe prevention thresholds in the name of the precautionary principle; aiming to prevent the appearance of any biological health implications linked to exposure to electric and magnetic fields, they have adopted very low exposure limits, notably in vulnerable zones (populated areas, hospitals, nurseries, schools), they consider that the limit values recommended by ICNIRP are relatively high and therefore a resulting exposure situation is potentially significant [19], [20].

ISSN: 2088-8708

As alternating current (AC) electric transporting power lines are counted among the main sources of electric and magnetic fields, which are all the more intense as the operating voltage of the overhead power line is increased and the current circulation there is significant. It becomes thus imperative to quantify and control the level of the electric and magnetic field radiated by these transmission power lines, in order to better protect public health and environmental safety from feasible hazards related to the power transmission lines [21]. Given the ongoing concerns of international society about the potentially long-term harmful impacts on the health of biological systems resulting from exposure to very low frequency magnetic fields produced by electricity transporting power lines; the latter is thus working to meet the challenge of finding solutions to effectively reduce ambient magnetic field levels.

Based on the above, this paper is presented with the aim to assess and reduce the magnetic induction profile created by an ultra-high-voltage overhead power line using a methodology of the physical principle of the Biot-Savart law and the theory of vector magnetic fields superposition [22]–[24]. Furthermore, an effective mechanism for improving the magnetic induction mitigation resulting from passive and active compensation loops is proposed, using the gray wolf optimizer (GWO) algorithm, which can provide a minimum total magnetic field in adjacency of ultra-high voltage (UHV) AC overhead transporting power lines.

The effect of magnetic compensation consists of inducing or injecting a current into a conductive loop placed in the immediate nearness of the electrical power transmission line. The secondary magnetic field resulting from the loop current partially or completely compensates the ambient primary magnetic field [25]–[29]. Determining the suitable location of the passive and active compensation loops coordinates and the quantities related to the mitigation process represent imposed constraints. To overcome these drawbacks, the meta-heuristic algorithms can be used to resolve such optimization problems. amongst the most common algorithms based on collective intelligence is the GWO. This algorithm was initially implemented by Mirjalili *et al.* it emulates The hierarchical structure and cooperative hunting mechanism of a society representing a gray wolf pack in the wildlife [30], [31]. In general, the GWO algorithm has proven to be quite effective on different types of functions, both in terms of accuracy of finding an extremum and in terms of convergence speed. Ultimately, the simulation results reached will be compared to those identified by the polarization ellipse technique for the magnetic induction analysis [32].

# 2. MODELING METHODOLOGY

This study proposes a quasi-static modeling technique to quantify and mitigate magnetic induction levels near an overhead very high voltage power line at power frequency. The idea behind our approach is to combine the fundamental principle of Biot-Savart's law with the usual theorem of superposition of vector fields from multiple overhead conductors with their images relative to the ground. The positioning of the denergized electric wires of the passive and active attenuation loops and the associated parameters was determined through an optimization process using the GWO algorithm to ensure high magnetic compensation. The novelty of this study lies in the combined application of these approaches to significantly and effectively reduce the effects of magnetic induction due to the proposed overhead transmission line.

5146 □ ISSN: 2088-8708

#### 2.1. Magnetic induction calculation

In magnetostatics, the Biot-Savart is largely applied to evaluate the magnetic induction at any point in space, created by a current element in a straight conductor of infinite length, as depicted in Figure 1. According to the superposition principle, the resulting magnetic flux density at point (*P*) is the vector sum of the elementary fields created by each current element. Therefore, the general expression for the resulting magnetic induction can be determined with (1) [33], [34]:

$$B = \frac{\mu_0 I}{2\pi r} \vec{e}_r \tag{1}$$

where, I is the current intensity passing across the conductor assumed to be infinitely long; r is the distance separating the current source and the considered point where the magnetic flux density is to be calculated;  $\vec{e}_r$  is a unit vector pointing in the direction of (r);  $\mu_0$  is the magnetic permeability of vacuum.

Three-phase UHV energy transport lines use several elementary conductors per phase, called bundles, in order to increase the energy transport capacity of the power transmission line; the amplitude of the current that passes through each phase conductor is distributed uniformly over the total number of elementary conductors constituting each phase conductor [35]. In UHV three phase power line circuits, a simple application of Biot–Savart law allows determining the overall magnetic flux density B due to all currents passing through the phase conductors of the power transmission line at any observation point [33], [34]. In field conditions, the height of the overhead conductor is greatly influenced by the variability of the terrain and the effect of atmospheric conditions (temperature, wind and ice load) on the conductor's sag value. Generally, to simplifying the calculation, the overhead transporting electrical energy conductors can be considered as straight, parallel to the others and parallel to a ground assumed to be perfectly flat, taking into account the notion of average height, see Figure 2, and it is calculated using the following relationship [36], [37]:

$$h_{ave} = h\left(\frac{2}{3}\right)_{max} \tag{2}$$

where,  $h_{max}$  represents the maximum height of the conductor at the sides of tower; S is the maximum sag of the conductor at the middle point of the conductor span.

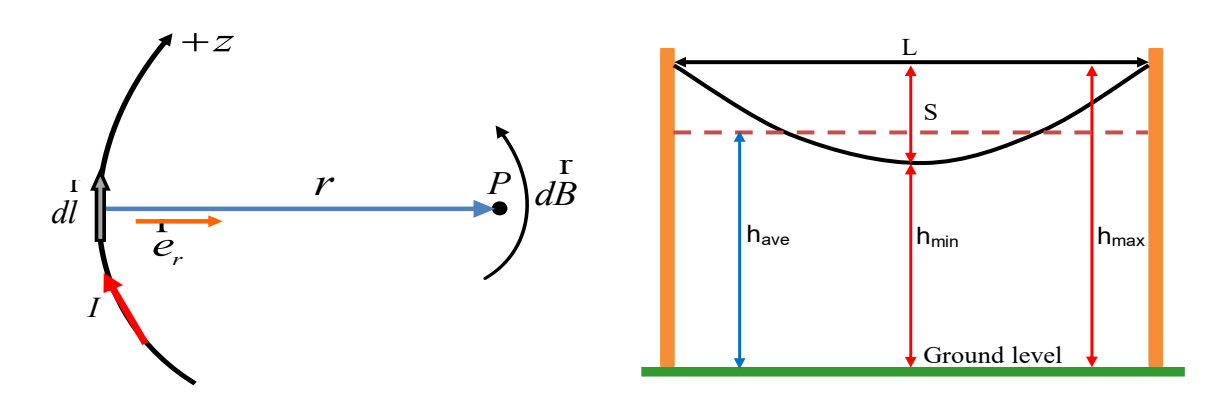


Figure 1. Descriptive schema of Biot-Savart law for magnetic field calculation

Figure 2. Simplified geometry of an overhead conductor suspended between two supports

It is important to note that these calculation procedures take into consideration the effect of the induced current in the ground wire and the ground effect, which can be represented by the images of the currents passing through the conductors situated at a depth in the soil combining the actual height of the conductors from the ground plus the depth of penetration of the currents which depends on the frequency of the source, as depicted in Figure 3 [36], [37].

In a two-dimensional (2D) rectangular coordinate system, the intensities of the horizontal and vertical components of the magnetic flux density created by the currents of the power line conductors at a desirable point P can be determined using the superposition principle according to the two equations expressed in the following [38]–[40]:

$$B_{x} = \frac{\mu_{0}}{2\pi} \sum_{i=1}^{n} I_{i} \left[ \frac{x_{j} - x_{i}}{d_{ij}^{2}} - \frac{x_{j} - x_{i}}{d'_{ij}^{2}} \right]$$

$$B_{y} = -\frac{\mu_{0}}{2\pi} \sum_{i=1}^{n} I_{i} \left[ \frac{y_{j} - y_{i}}{d_{ij}^{2}} - \frac{y_{j} + y_{i} + D_{e}}{d'_{ij}^{2}} \right]$$
(3)

where,  $I_i$  are the electric currents circulating across the conductors of the power line; n is the total number of conductors in the electrical transmission line;  $d_{ij}$  is the distance separating each conductor and the considerable point P (the point where it wants to calculate the magnetic induction);  $d'_{ij}$  is the distance separating each image conductor and the considerable point (P) as shown in Figure 3;  $D_e$  represents the complex penetration depth of the electric current return in the ground, it is estimated by the following expression [36], [37]:

$$D_e = \sqrt{2} \sqrt{\frac{\rho_S}{\pi \mu_0 f}} e^{-j\frac{\pi}{4}} \tag{4}$$

where,  $\rho_s$  is the resistivity of the soil, expressed in  $(\Omega.m)$ ; f is the frequency of the AC power supply defined in (Hz); j is the fundamental imaginary unit.

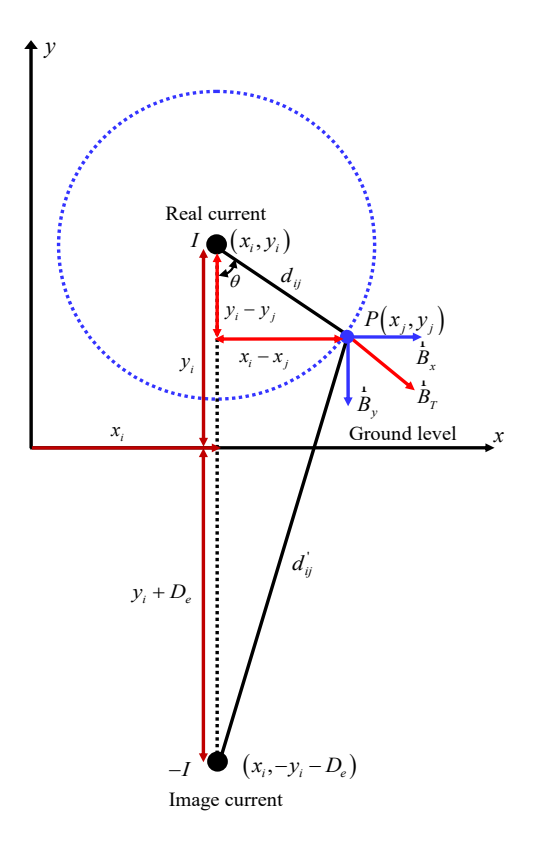


Figure 3. Magnetic field generation around a courant flowing through a conductor

The resulting amplitude of magnetic flux density intensity is accessed by summing the both components provided above, as outlined by the following relationship [36], [37]:

$$|B_t| = \sqrt{B_x^2 + B_y^2} \tag{5}$$

In the case of a sinusoidal variation over time; the intensity of the magnetic flux density can be displayed by a quantity representing a phasor vector which varies over time due to the variation of the phasor of the electric current that is effectively transmitted in the conductor. The current phasor passing through the conductor associated with a sinusoidal variation is expressed with real and imaginary part, as [41]:

$$[I_i] = [I_i]_{re} + j[I_i]_{im} \tag{6}$$

The expression for the resulting magnetic induction using phasor notation can be written as (7):

$$B_t = |B_t|e^{j\varphi_{B_t}} \tag{7}$$

where,  $|B_t|$  is the intensity of magnetic flux density;  $\varphi_{Bt}$  is the phase angle of the magnetic flux density, it is calculated as (8):

$$\varphi_{B_t} = \arctan\left(\frac{B_y}{B_x}\right) \tag{8}$$

Since the influence of the value of the induced currents in the ground wires deriving from the overhead transmission line currents is taken into account in magnetic flux density calculating; the quantity of these currents can be found as [36], [37]:

$$\begin{bmatrix} I_a \end{bmatrix} = - \begin{bmatrix} Z_{aa}^{-1} \end{bmatrix} \begin{bmatrix} Z_{ap} \end{bmatrix} \begin{bmatrix} I_p \end{bmatrix} \tag{9}$$

where,  $I_g$  indicate the AC electric induced currents in the ground wires;  $I_p$  represent the nominal currents of the phase conductors;  $Z_{gg}$  describe the self-impedances of ground wires;  $Z_{gp}$  represent the mutual impedances between the phase conductors and the ground wires. It is possible to estimate the self and mutual impedances per unit length using the analytical approach of the simplified Carson-Clem theorem; as shown in the following expressions respectively [36], [37]:

$$Z_{gg} = R_g + \frac{\mu_0 \omega}{8} + j \frac{\mu_0 \omega}{2\pi} \left[ \frac{1}{4} + ln \left( \frac{D_e}{r_g} \right) \right]$$

$$Z_{gp} = \frac{\mu_0 \omega}{8} + j \frac{\mu_0 \omega}{2\pi} ln \left( \frac{D_e}{d_{gp}} \right)$$
(10)

where,  $R_g$  is the AC resistance of ground wire in  $[\Omega/m]$ ;  $d_{gp}$  is the distance separating the phase conductor from the ground wire in [m]  $r_g$  is the geometrical radius of ground wire in [m]. The Carson-Clem's principle can be used when the separation distance between phase conductors is little then 15% of corresponding soil recovery location  $D_e$ .

# 2.2. Magnetic induction mitigation

The biological impacts of low-frequency electromagnetic fields on the population health have remained a major preoccupation of the international society for several decades. The electric field is easily stopped by all types of materials; while the magnetic field is able to pass through most materials, even the human body, and cannot be stopped. Protection consists of staying away from the source or using shielding strategies [42].

In order to minimize potential effects associated with very low frequency magnetic field radiation, the most common reduction technique in magnetic field shielding of UHV overhead transmission lines is the implementation of an effective compensation system. The principle of this technique is based on the insertion of a conductive loop made up of two conductors connected together; and is installed neatly under the phase conductors in an appropriate position of the area of interest to be protected. This closed loop is intended to produce an auxiliary magnetic field which opposes the original magnetic field, in order to compensate it partially or totally, as explained in Figure 4. This compensation of magnetic flux density is produced either by an induced current by the phase conductors (passive compensation), or by an injected current by a secondary power source (active compensation) [25]–[31]. It is important to mention that this compensation system does not only apply to new lines, but can also be used for existing lines; they can be used separately or together if necessary.

# 2.2.1. Passive loop compensation

This strategy involves installing a passive loop consisting of two conductors forming a closed circuit properly established between the phase conductors of the overhead power line and the ground level. According to Faraday's law of magnetic induction, the latter, resulting from the magnetic field of the power line, produces a magnetic flux, the temporal variation of this magnetic flux through the passive loop produce an electromotive force (EMF), which causes the circulation of an induced current which in turn will produce

П

an induced magnetic induction opposite to that of the conductors of the line, in order to partially compensate for it [43]–[49]. The EMF induced in the compensation loop is represented as the opposite derivative with respect to time of the magnetic flux through this closed loop; it is expressed by the relation [43]–[49]:

$$e(t) = -\frac{d\phi_l}{dt} \tag{11}$$

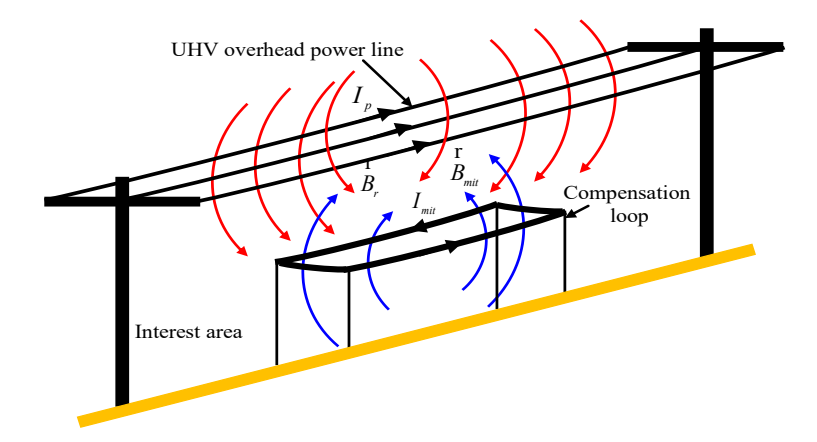


Figure 4. Installation of a conductive compensation loop under the UHV overhead transmission line

The negative sign (-) describes the behavior of Lenz's law, the electromotive force tends to oppose the variation in magnetic flux, it identifies the direction of the AC induced current circulation in the compensation loop. The induced electrical voltage across this compensation closed loop can be estimated using the following [43]–[49]:

$$V_{ind} = -j\omega\ell\phi_l \tag{12}$$

where,  $V_{ind}$  is the AC induced voltage;  $\omega$  expresses the angular frequency in (rad/s);  $\ell$  is the passive loop length;  $\theta_l$  is the magnetic flux in the closed loop conductors. As the passive compensation loop is arranged horizontally under the phase conductors of the power line, and consequently, only the vertical component of the magnetic induction which is perpendicular to the plane of this passive loop contributes to the value of the magnetic flux. The magnetic flux  $\theta_l$  through the passive loop can be calculated using the formula [43]–[49]:

$$\phi_l = \int_{x_1}^{x_2} \vec{B}_y d\vec{x} \tag{13}$$

The two conductors constituting the passive loop are located at the coordinates  $(x_1, x_2)$  and  $(y_1, y_2)$  as indicated in Figure 5. By integration of the vertical magnetic field through the coordinates of the closed loop conductor's, the magnetic flux is expressed as [43]–[49]:

$$\phi_l = -\frac{\mu_0 \ell}{4\pi} \sum_{i=1}^n I_i \ln \frac{\left[ (x_2 - x_i)^2 + (y_i - y_2)^2 \right] \left[ (x_1 - x_i)^2 + (y_i + y_1 + D_e)^2 \right]}{\left[ (x_2 - x_i)^2 + (y_i - y_1)^2 \right] \left[ (x_2 - x_i)^2 + (y_i + y_2 + D_e)^2 \right]}$$
(14)

where,  $(x_i, x_i)$  are the orthogonal coordinates of the conductors of the power line;  $I_i$  presents the currents circulating in the conductors of the power line. The total impedance value of the passive loop is presented by a resistance in series with an inductance and an electrical capacitance; it is given by the following formula [50], [51]:

$$Z_l = \sqrt{R_l^2 + \left(\omega L_l - \frac{1}{\omega C_l}\right)} \tag{15}$$

In general, the capacitance in the passive loop is integrated in series with the inductance in order to cancel part of the inductive reactance, aiming to increase the current intensity passing through the conductors of the closed loop; which provides effective magnetic field compensation. The self-inductance of the passive closed loop is determined as [43]–[49]:

$$L_l = 4 \times 10^{-7} \times \ell \times \ln\left(\frac{s_l}{r_l}\right) \tag{16}$$

where,  $r_1$  is the radius of passive loop conductor;  $s_1$  is the distance separating the two conductors of the conductive loop. The current intensity through the conductors of the compensation loop is determined by the formula as [43]-[49]:

$$I_{loop} = \frac{v_{ind}}{Z_l} \tag{17}$$

This induced current will create a magnetic induction which opposes that generated by the currents of the source, according to (3) mentioned above. The resulting magnetic induction is obtained by summing the vectors of the initial magnetic induction and that of the compensation loop, as indicated in the following relation [43]–[49]:

$$\vec{B}_{res} = \vec{B}_t + \vec{B}_{loop} \tag{18}$$

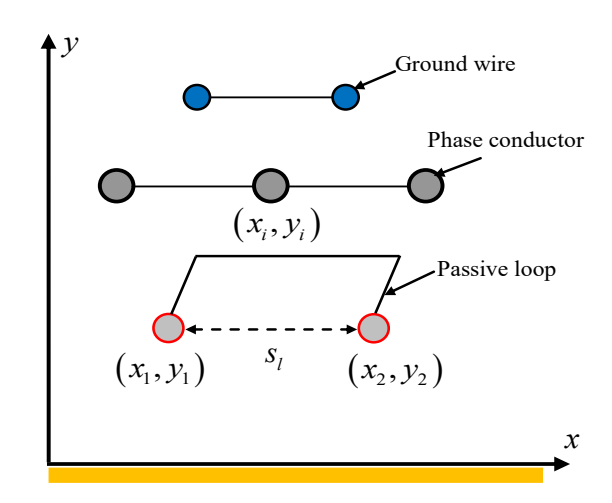


Figure 5. Orthogonal coordinates of the power line conductors and passive closed loop

## 2.2.2. Active loop compensation

In this compensation procedure, a current is generated from an external power source consisting of an active feedback loop guided by a measuring sensor that controls the current value circulating in the both loop conductors and detects the variation of the compensating magnetic induction created which interacts with that generated by the currents of the power line in order to partially or perfectly compensate in the zone to be protected [51]–[56]. The value of the current to be injected must be carefully calculated in order to obtain significant compensation. There are two different methods to determine the current of the source to be injected, either using empirical formulas, or by a calculation algorithm which makes it possible to adjust the coil current and compensate the ambient magnetic induction [51]–[56].

For a designing loop, according to the empirical relation; the components real and imaginary of injecting current are calculated according to the (19) and (20) defined written as [56]:

$$Re\left[I\left[\frac{-b_{x}Re[B_{o}]_{x}-b_{y}Re[B_{o}]_{y}}{b_{x}^{2}+b_{y}^{2}}\right] Im\left[I\left[\frac{-b_{x}Im[B_{o}]_{x}-b_{y}Im[B_{o}]_{y}}{b_{x}^{2}+b_{y}^{2}}\right]\right]$$
(19)

where  $[B_0]_x$  and  $[B_0]_y$  are the both components of the starting magnetic induction due to the overhead power line at the destined point;  $b_x$  and  $b_y$  are the both components of the magnetic induction emitted at a similar position across the active compensation loop, assuming the input current in this loop has a magnitude I = IA and a phase  $\theta = 0$ . Similarly, to (18) noted above, the resulting magnetic induction is equal to the sum of the magnetic induction vectors of the overhead power line and that established by the active compensation

loop. To quantify the performance of magnetic induction attenuation carried out in a specified region; it is important to take into account the reduction factor (or shielding factor), which is the ratio of magnetic induction without the compensation effect to the magnetic induction with compensation effect; it is obtained from the following expression [46], [55], [57]:

$$RF = \frac{B_0}{B_{res}} \tag{20}$$

where,  $B_0$  is the magnetic induction without shielding;  $B_{res}$  is the magnetic induction with shielding.

#### 3. GREY WOLF OPTIMIZER

GWO is an algorithm initially developed by Mirjalili in 2014, based on how a pack of gray wolves hunts in the wild. This pack includes alpha wolves ( $\alpha$ ), beta wolves ( $\beta$ ), delta wolves ( $\delta$ ), and omega wolves ( $\omega$ ), each with a specific social role and hierarchy [30]. The hunting process involves tracking, trapping, and then attacking prey. In the GWO mathematical model, the primary solution is alpha, followed by beta and delta, while the remainder is omega. The prey encirclement behavior is modeled using mathematical relationships that mainly involve coefficient vectors and position vectors. The core pursuit of the hunt is carried out by alpha wolves, with secondary participation from beta and delta wolves. The potential location of the prey is evaluated using the best solutions, and the other wolves adjust their positions accordingly. The final stage is the actual attack and capture of the prey, which occurs when the wolves completely stop moving. Exploration and exploitation are balanced by adaptive values [58]–[62]. The environmental behavior of all stages of the predation act can be effectively modeled using the following set of equations:

$$\vec{D} = \left| \vec{C} \vec{X}_p(t) - \vec{A} \vec{X}(t) \right| \tag{21}$$

$$\vec{X}(t+1) = \vec{X}_p(t+1) - \vec{A}\vec{D}$$
 (22)

where;  $\vec{X}_p$  and  $\vec{X}$  are the possible location vectors of the prey and a grey wolf respectively;  $\vec{A}$  and  $\vec{C}$  are coefficient vectors, t is the iteration number. The coefficient vectors  $\vec{A}$  and  $\vec{C}$  are evaluated as [58]–[62]:

$$\vec{A} = 2\vec{a} \times \vec{r_1} - \vec{a} \tag{23}$$

$$\vec{C} = 2 \times \vec{r_2} \tag{24}$$

where;  $\vec{a}$  is a coefficient vector which gradually decreases from 2 to 0 over the course of iterations in GWO algorithm;  $\vec{r}_1$  and  $\vec{r}_2$  are random vectors with values ranging in the interval [0-1].

Regarding the (25)-(27) governing the mathematical model of the grey wolf hunting process, it is assumed that Alpha  $\alpha$ , Bêta  $\beta$  and Delta  $\delta$  wolves bring greater knowledge about the likely seat of the prey; they direct the search process and the Oméga  $\omega$  wolves adjust their emplacements, based on the sites of the three most skillful wolves, this can be explained in the following form [58]–[62]:

$$\vec{D}_{\alpha} = \left| \vec{C}_{1} \vec{X}_{\alpha}(t) - \vec{X}(t) \right| \vec{D}_{\beta} = \left| \vec{C}_{2} \vec{X}_{\beta}(t) - \vec{X}(t) \right|, \vec{D}_{\delta} = \left| \vec{C}_{3} \vec{X}_{\delta}(t) - \vec{X}(t) \right|$$
(25)

$$\vec{X}_{1} = |\vec{X}_{\alpha}(t) - \vec{A}_{1}\vec{D}_{\alpha}| \vec{X}_{2} = |\vec{X}_{\beta}(t) - \vec{A}_{2}\vec{D}_{\beta}| \vec{X}_{3} = |\vec{X}_{\delta}(t) - \vec{A}_{3}\vec{D}_{\delta}|$$
(26)

$$\vec{X}(t+1) = \frac{\vec{X}_1 + \vec{X}_2 + \vec{X}_3}{3} \tag{27}$$

where,  $\vec{X}_{\alpha}(t)$ ,  $\vec{X}_{\beta}(t)$  and  $\vec{X}_{\delta}(t)$  are the positions vectors of the grey wolves  $\alpha$ ,  $\beta$  and  $\delta$  at  $k^{th}$  iteration respectively,  $\vec{A}_1$ ,  $\vec{A}_2$  and  $\vec{A}_3$  are adaptive vectors. In GWO algorithm, exploration (search for prey) and exploitation (attacking prey) are two opposite phases. The random vector  $\vec{a}$  mentioned in (23) is considered as a basic factor controlling exploration and exploitation; it declines in a linear manner from the value 2 to 0 over the generations and is calculated as shown in the [58]–[62]:

$$a = 2 - t \times \frac{2}{Max_{iter}} \tag{28}$$

where; t is the current iteration and  $Max_{iter}$  is the maximum number of literation.

As a result, the equivalent quantity of vector  $\vec{A}$  also changes in the range [-a, a]. Possible solutions represent wolves approaching the prey at  $|\vec{A}| > 1$  and moving away from it at  $|\vec{A}| < 1$ ; when  $|\vec{A}| = 1$ , there is no convergence towards the desired result. All the basic stages of the GWO algorithm are concisely represented in the pseudo-code indicated in Table 1 [63], [64]:

Table 1. Pseudo-code of the GWO optimization algorithm

```
Pseudo-code of the GWO algorithm
1: Generate randomly an initial population of
2: Initialize the values of a=2, A, C and Max iter
3: Evaluate the fitness function of each member of the
population, X\alpha, X\beta and X\delta
4: While (t< Max iter) do
5:
    For each search agent do
        Update the location of all wolves (using (25), (26)
6:
and (27)
7:
          Update A, C (using (23) and (24)
          Update a (using (28))
9:
    end for
       Calculate Fitness value of all search agents
10:
11:
        Update X\alpha, X\beta, X\delta
13: end while
14: Return the best solution X\alpha
```

An optimization of maximization of an objective function is designed, in order to decide the location of the compensation loop conductors coordinates, as well as the values of different elements associated with the compensation strategy, to efficiently reduce the magnetic induction in the area to be protected. The used objective function in this maximization process is based on the square root of the distinction between the initial magnetic induction strength at a given point and its intensity after compensation at the same point. This function can be expressed mathematically using the formula shown [65]:

$$OF = -\sqrt{(B_t - B_{res})^2} \tag{29}$$

where,  $B_t$  is the magnetic induction quantity before the compensation design at a designated point;  $B_{res}$  is the magnetic induction quantity after the compensation, based on all optimized quantities at the same point. The negative sign linked with the beginning of the objective function indicates that the designed optimization procedure is for the function maximization.

# 4. ELLIPTICAL POLARIZATION

In a permanent sinusoidal regime, each sinusoidal quantity at constant frequency is a phasor which can be expressed by a magnitude and a phase angle. The extremity of the vector of the resultant magnetic induction  $\vec{B}$  due to three-phase power line traces at a fixed observation point an ellipse as a function of time as the vector rotates. This property represents an elliptical polarization state that describes the change with time in the amplitude and phase angle of the vector as reflected in Figure 6.

Generally, the ellipse equation is determined by orthogonal components, by projection onto the orthogonal axes of the (x, y) plane, each vector can be decomposed into two components, real and imaginary, as noted [66]–[71]:

$$\vec{B}_x = (B_{rx} + jB_{ix})\vec{u}_x$$

$$\vec{B}_y = (B_{ry} + jB_{iy})\vec{u}_y$$
(30)

The peak value of magnetic induction is reached by the projection of the instantaneous rotation vectors along the two axes. The magnitude of the magnetic induction, in a direction determined by an orientation angle  $\varphi$  can be expressed as [66]–[71]:

$$B_{x} = (B_{rx}\cos \varphi + B_{ix}\sin\varphi)$$

$$B_{y} = (B_{ry}\cos\varphi + B_{iy}\sin\varphi)$$
(31)

The square of the magnetic induction is equal to the sum of the squares of the complex vectors along two axes x and z; It is given by the following relation [66]–[71]:

$$B_m^2 = B_x^2 + B_y^2 (32)$$

The ellipse function which presents the magnetic induction passes through a maximum and a minimum when its first derivative is null. This can be expressed mathematically as [66]–[71].

$$\frac{dB_j^2}{d\varphi} = 0 ag{33}$$

Indeed, the resulting magnetic induction at a known point is equal to the sum of the squares of two solutions concerning the extreme modules of two semi-axes, it is defined as [66]–[71]:

$$B_{\rm res} = \sqrt{B_{\rm max}^2 + B_{\rm min}^2} \tag{34}$$

where,  $B_{max}$  and  $B_{min}$  are the semi-major and semi-minor Rms values of magnetic induction axial ellipse, respectively, as shown in Figure 6.

Consider a segment of a 750 kV three-phase transmission power line with a symmetrical horizontal phase sequence arrangement with two earth wires. The arrangement and geometric coordinates with the average height of the conductors of the transmission line relative to the suspension pylon are illustrated in Figure 7 [71]. Each phase conductor is bundled with four sub-conductors, the power transferred for this transmission line is considered equal to S=4000 MVA. The earth is supposed to be uniform of electrical resistivity 100  $\Omega$ /m; the normal frequency of 50 Hz, the direct current (DC) resistance for phase conductor is 0.0684  $\Omega$ /km, while for the earth wire is 0.643  $\Omega$ /km. Concerning the geometric parameters of the compensation loop, a rectangular conductive loop with a radius equal to 1.12 mm and a resistance per unit length with a value of 0.225  $\Omega$ /km; the length of the closed loop formed by the two conductors located in the area to be protected is equal to 1000 m.

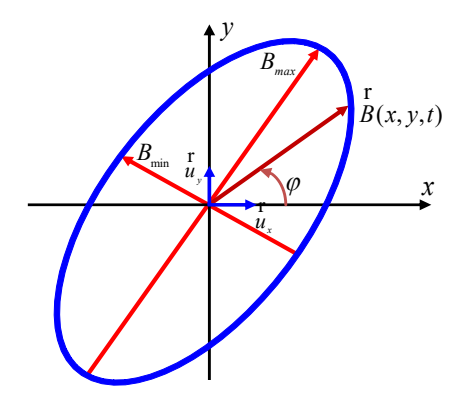


Figure 6. Components of elliptically polarized magnetic induction

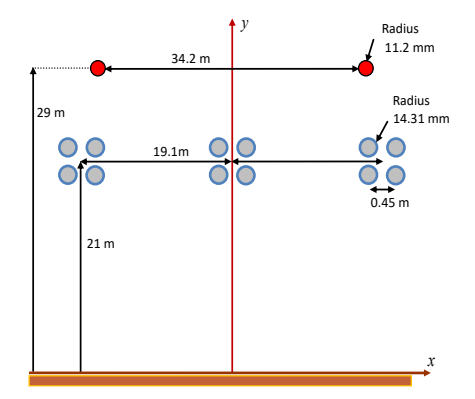


Figure 7. Geometric configuration of a 750 kV single-circuit horizontal overhead power line

# 5. RESULTS AND DISCUSSION

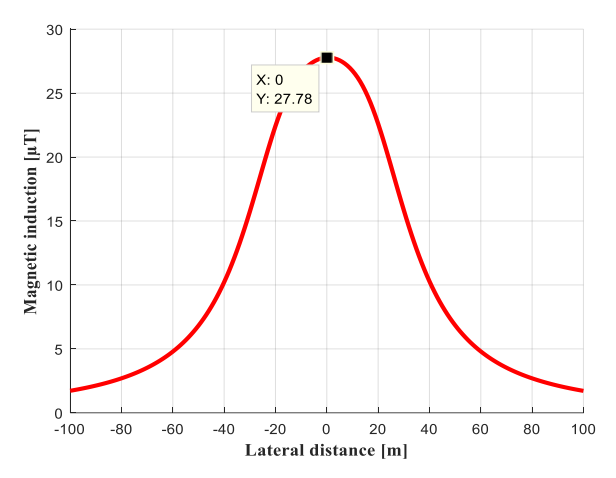
The first step of this study involves the magnetic induction computation generated in the vicinity of an extreme high voltage line of 750 kV. Initially, as this power line is designed to deliver an apparent power of 4000 MVA, the value of the modulus of the current passing through the phase conductor is 3079.20 A, the currents induced in the earth wires according to (9) mentioned above, in order to take them into account in the contribution to the calculation of magnetic induction are respectively:

$$I_{g1} = 495.07e^{j(158.46)^{\circ}}, I_{g2} = 496.2e^{j(-23.92)^{\circ}}$$

The lateral profile of the magnetic induction intensity of this power line geometry studied at 1 m above the ground is indicated in Figure 8, it reaches its maximum under the central phase conductor with a

value of 27.78 μT; then it gradually decreases as the distance increases from this power line center on both sides of the corridor. In particular, it can be stated that the lateral variation of the magnetic induction reflects an approximately Gaussian shape.

The distribution of the magnetic induction contour lines around the conductors of the power line in space (x, y) is presented in Figure 9. It can be remarked that the values of the magnetic induction are intense in the immediate vicinity of the circumference of conductors, and then gradually decrease as it moves away from the current source. It can be deduced that the magnetic induction is directly linked to the distance between the observation point coordinates and the current-carrying conductor. As separating distance increases, the magnetic induction decreases strongly.



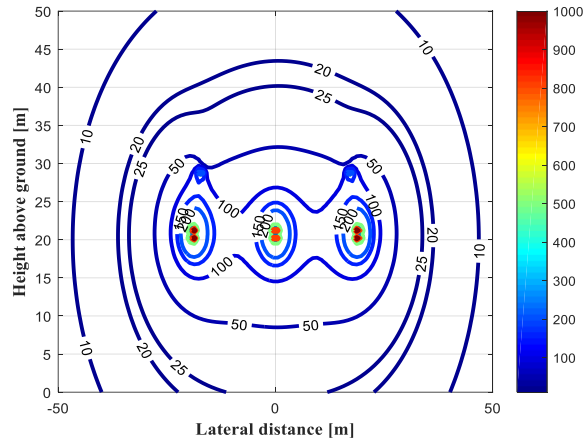


Figure 8. Lateral profile of magnetic induction at 1m above the ground level

Figure 9. Contour lines of magnetic induction distribution in XY plane

The temporal evolution of the magnetic induction vector at the observation point (x=0 m, y=1m) is shown in Figure 10. It can be seen that the peak value is obtained at time t = 0.0035 (s) for an argument  $\varphi = 22.04^{\circ}$ . Also, the instantaneous values of the magnetic induction phasor components (modulus and argument) vary both in amplitude and sign within a cycle.

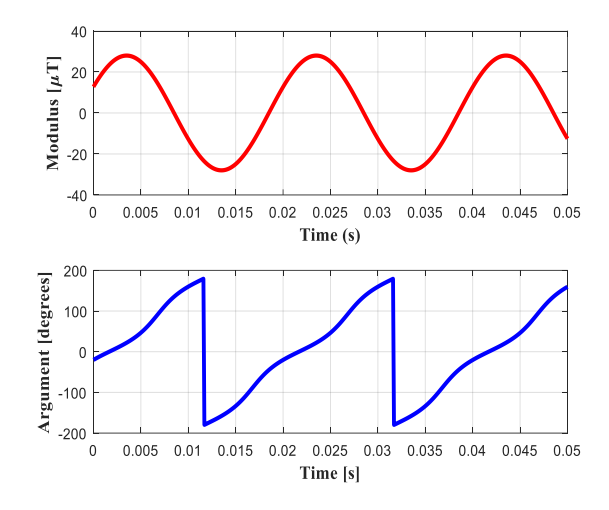


Figure 10. Temporal variation of the magnetic induction vector over time

The second step consists of implementing a mitigation procedure to reduce the emission of magnetic induction in the area of interest. In order to obtain significant compensation to minimize the level of magnetic induction exposure, it is necessary to apply the adopted optimization algorithm to determine the optimal

location of the compensation loop conductors and the associated parameters, such as the compensation capacitance of the passive loop and the current to be injected into the active loop. The initial parameters used for the adopted GWO algorithm are defined as: the number of agents is 20, the coefficient (a) is contained in the range [0, 2], the random vectors  $r_1$  and  $r_2$  are in the interval [0, 1], the maximum number of iterations is set to 100.

The evolution of the objective function specified in (29) during iterations for both types of compensation is shown in Figure 11. The values of the objective function during the optimization process gradually increase in order to maximize it, after a number of iterations, the algorithm converges to the best values according to the search space. After evaluating the objective function; the obtained results representing the optimal values of the decision variables indicated in the objective function which are the coordinates of the loop conductors; the compensation capacitance and the injected current are presented respectively in Figures 12, 13, and 14; where it is clearly observed that the algorithm converges fastly towards these best solutions after a limited number of iterations.

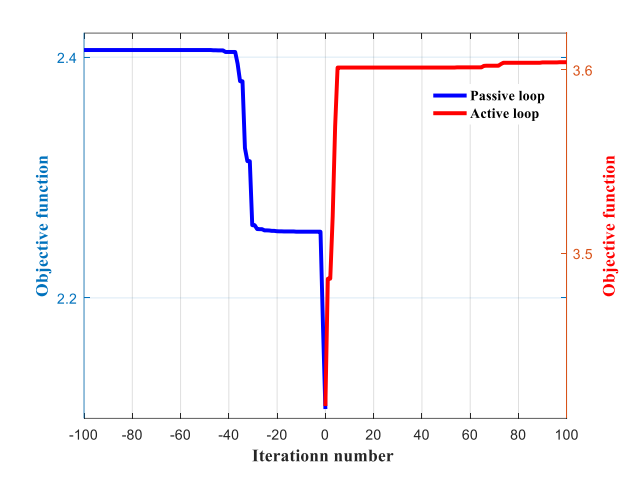
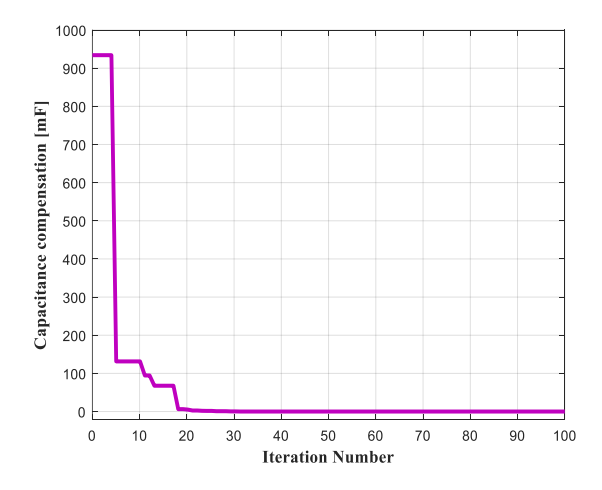


Figure 11. Objective function variation according to iterations number

Figure 12. Convergence to the optimal coordinates values of compensation loops



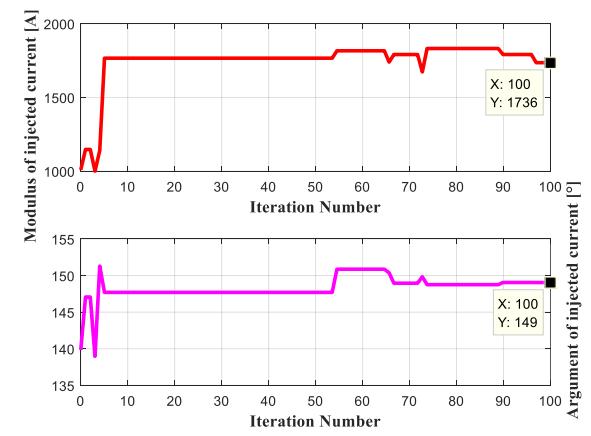


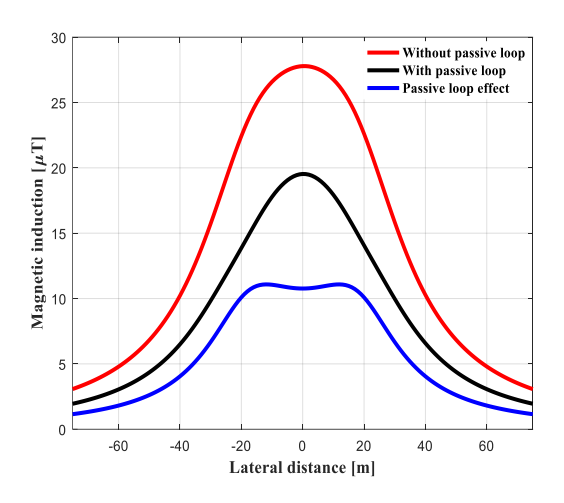
Figure 13. Convergence of the compensation capacitance value for passive loop

Figure 14. Convergence of module and argument values of the current to be injected into the active loop

Figure 15 represents the lateral distribution of magnetic induction at 1m above ground level without and with the passive loop. By comparing the calculated values with and without the passive loop along the right-of-way, it can be observed that the magnetic induction is decreased at all points along the power line corridor. However, this passive loop decreases the magnetic induction by a rate of 29.7% of its maximum value.

5156 □ ISSN: 2088-8708

Figure 16 provides the empirical assessment of module and argument of the current to be inserted in the active loop positioned in coordinates optimized by the GWO algorithm, according to the lateral distance with a height of 1m at ground level. It can be clearly seen that the current modulus presents a symmetrical graphic illustration with respect to the center point, starting from this point, the modulus decreases until reaching a critical value; from where it comes to increase rapidly then slowly to maintain a convergent value. For the argument, starting from the left side of the right of way, the argument increases very slightly until reaching a maximum value; then it decreases slightly passing through the center to reach a minimum value, from there, it increases very slowly in order to maintain a similar value.



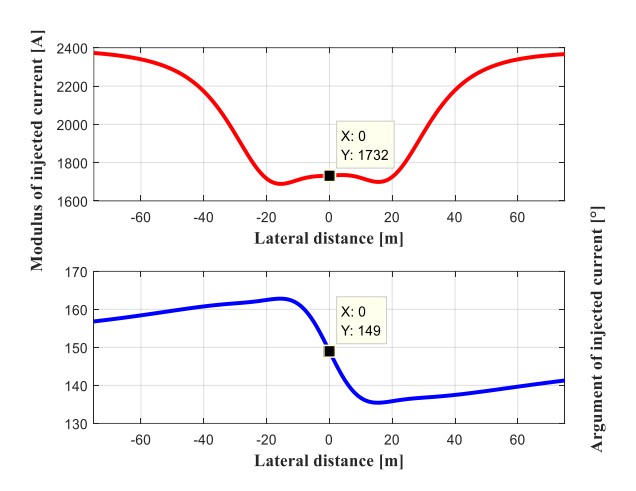


Figure 15. Profile of magnetic induction at 1 m above ground level without and with the passive loop

Figure 16. Empirical calculation of the module and argument of the current to be injected into the active loop

A comparison can be made between the value calculated using the empirical law indicated in (19) and that optimized by GWO algorithm concerning the module and the argument of the current to be injected into the active loop at the coordinate point (x = 0 m, y = 1 m). Table 2 summarizes the results, which can be considered very close, which proves the rigorous accuracy and high performance of the empirical law.

Table 2. Comparison between the calculated and optimized current to be injected into the active loop

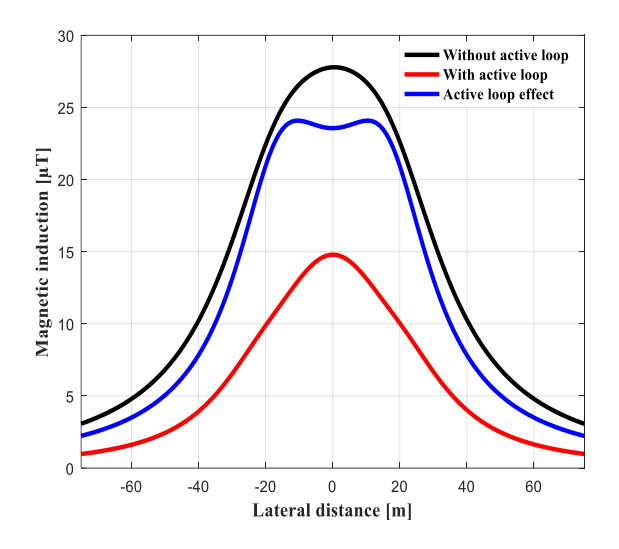
Injected current into	Calculated value by	Optimized value by
active loop	empirical formula	GWO algorithm
Module (A)	1732.3	1735.7
Argument (°)	149.04	149.12

Figure 17 illustrates the lateral distribution of magnetic induction at 1 m above ground level, with and without the presence of the active loop. It can be noted that the maximum value of magnetic induction obtained at the power line center decreases by a percentage of 53.24%. In general, with the presence of the active loop the magnetic induction undergoes a significant reduction at all points along the right-of-way of the power line. The active compensation loop provides a better reduction of magnetic induction than the passive loop.

Figure 18 describes the effectiveness of shielding with passive and active compensation loops expressed by the reduction coefficient of the magnetic induction; the presence of the compensation loop underneath the conductors of the overhead power line allows reducing the magnetic induction values. In the case of passive shielding, the reduction coefficient varies between the values 1.42 and 1.63; while in the case of active shielding, it ranges between the values 1.9 and 3.15. Therefore, the active loop has a greater compensation effect than the passive loop; it considerably reduces the magnetic induction at all points of the power transmission line right of way.

The last step is to ensure the reliability and accuracy of the results obtained by the adopted method. In order to best perform this validation, the polarization ellipse method has been proposed. Figure 19 depicts the profiles of the resulting magnetic induction and the maximum and minimum components along the x and

y axes obtained with the ellipse approach calculated at 1 m height above the ground. It is clear from this figure that these graphs have a symmetrical shape where the maximum values are obtained directly under the central phase conductor; then they decrease rapidly as the distance from the symmetry center increases. To illustrate this, Figure 20 shows the geometric shape obtained at the point (x = 0 m, x y = 1 m), which shows the extreme values of the magnetic induction components, while the tip of the magnetic induction vector rotates over time to trace an elliptical polarization shape in the XY plane.



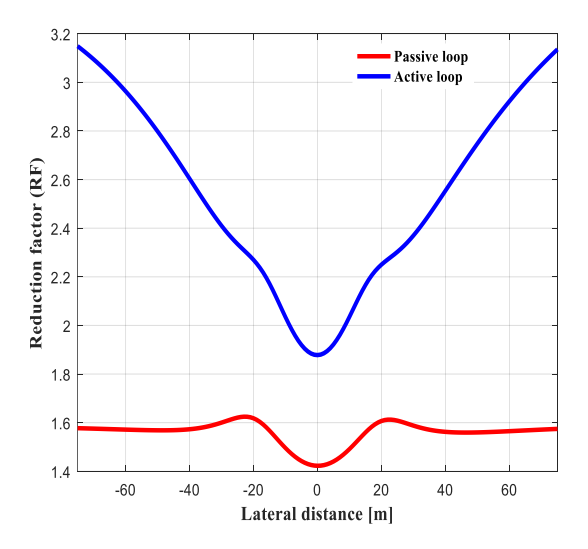
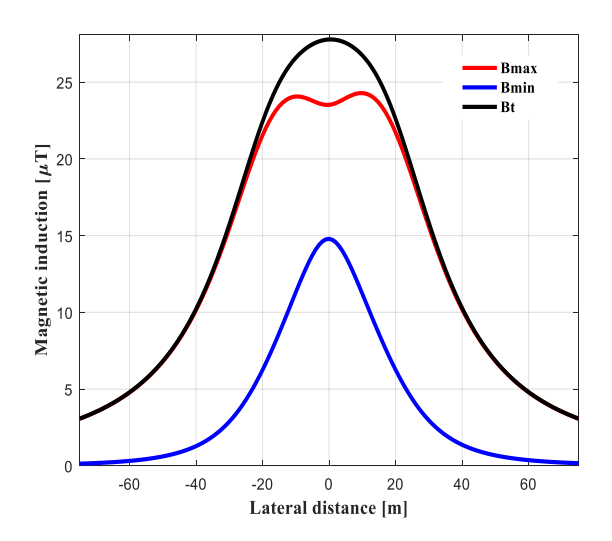
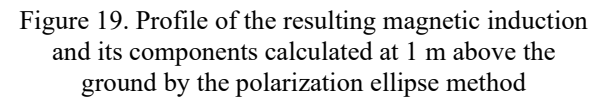


Figure 17. Profile of magnetic induction at 1 m above ground level without and with the active loop

Figure 18. Active and passive shielding reduction

The lateral profiles of the magnetic induction for the same power line geometry without and with the passive and active compensation loops calculated by the ellipse method at 1 m above ground level are illustrated in Figure 21. Comparing the graphs in this figure with those presented in Figures 10, 17, and 19, it can be clearly noted a very good agreement between the values obtained and those taken from the previous figures, with a maximum relative error of about 1.05%, which can be neglected. Therefore, this comparison allows to ensure the efficiency and accuracy of the adopted method in order to confirm its validation.





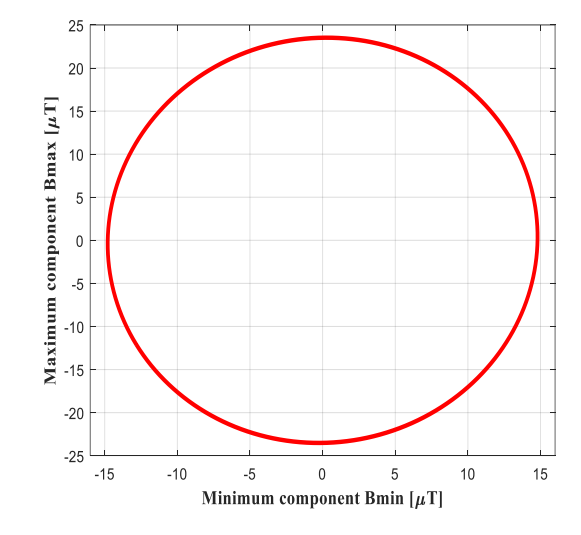


Figure 20. Polarization ellipse described by the magnetic induction vector at point (x=0 m, y=1 m)

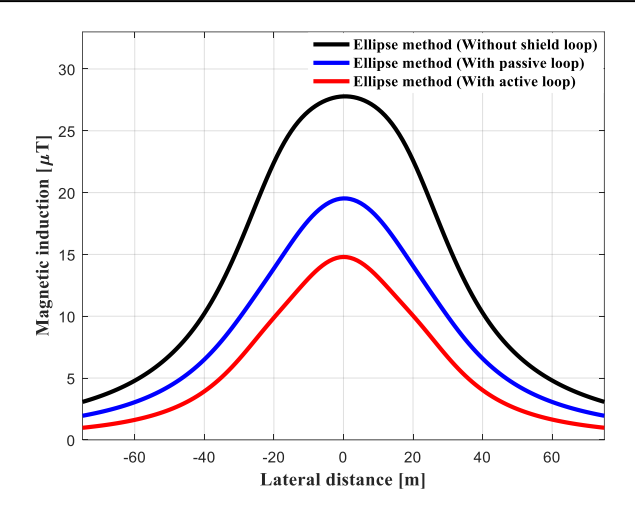


Figure 21. Magnetic induction profiles without and with passive and active loops obtained by the polarization ellipse method

#### 6. CONCLUSION

The necessity to quantify the magnetic induction levels generated by nearby UHV power transmission lines has become an extremely paramount task for human health and environmental reasons. This study focuses on a two-dimensional (2D) mathematical analysis of a quasi-static simulation of magnetic induction created by a 750 kV transmission power line, based on a methodology combining the Biot-Savart law and the superposition theorem of elementary fields; as well as addressing the mitigation procedure caused by passive and active compensation loops. An optimization technique based on the GWO is adopted, in order to determine the optimum quantities of optimization parameters concerning the position of the compensation loop wires and the associated parameters that provide better compensation. From the presented results, it is evident that the peak value of the magnetic induction is recorded at the point of symmetry located under the central phase conductor of the transmission line configuration, as one moves away from this position, the magnetic induction progressively declines due to increasing side distance from the symmetry center. After identifying the optimal parameters with the GWO optimization algorithm, the attenuating effect of the passive and active conductive loops installed below the phase conductors of the transmission line configuration is demonstrated. The results also indicated that the optimum design of both passive and active compensation loops ensures sufficient efficiency and effectiveness to reduce the magnetic induction levels along the corridor of ultra-high-voltage power lines. Therefore, the active loop is considered as a reliable, more efficient and more rigorous mechanism in compensating the magnetic induction in a zone of substantial interest; it offers a higher shielding coefficient than the passive loop. Finally, a fair comparison was made between the simulation results determined using the established method and those provided by the elliptical polarization technique; the graphs of both methods are almost identical, which ensures the efficiency and accuracy of the present method.

# **ACKNOWLEDGEMENTS**

The authors would like to thank the head and staff of Laboratory for Analysis and Control of Energy Systems and Electric Systems, LACoSERE, University of Amar Telidji, Laghouat (03000), Algeria.

## REFERENCES

- [1] A. A. Mir, M. Alghassab, K. Ullah, Z. A. Khan, Y. Lu, and M. Imran, "A review of electricity demand forecasting in low and middle income countries: the demand determinants and horizons," *Sustainability*, vol. 12, no. 15, p. 5931, Jul. 2020, doi: 10.3390/su12155931.
- [2] M. Khanna and N. D. Rao, "Supply and demand of electricity in the developing world," Annual Review of Resource Economics, vol. 1, no. 1, pp. 567–596, Oct. 2009, doi: 10.1146/annurev.resource.050708.144230.
- [3] A. Ahlbom *et al.*, "Possible effects of electromagnetic fields (EMF) on human health opinion of the scientific committee on emerging and newly identified health risks (SCENIHR)," *Toxicology*, vol. 246, no. 2–3, pp. 248–250, Apr. 2008, doi: 10.1016/j.tox.2008.02.004.
- [4] F. Barnes and J. E. R. Freeman, "Some thoughts on the possible health effects of electric and magnetic fields and exposure guidelines," Frontiers in Public Health, vol. 10, Sep. 2022, doi: 10.3389/fpubh.2022.994758.
- [5] S. Singh and N. Kapoor, "Health implications of electromagnetic fields, mechanisms of action, and research needs," Advances in

П

- Biology, vol. 2014, pp. 1–24, Sep. 2014, doi: 10.1155/2014/198609.
- A. Razek, "Biological and medical disturbances due to exposure to fields emitted by electromagnetic energy devices—a review," [6] Energies, vol. 15, no. 12, p. 4455, Jun. 2022, doi: 10.3390/en15124455.
- W. G. IGRE, "Electric and magnetic fields produced by transmission systems. description of phenomena--practical guide for calculation." CIGRE Paris, 1980.
- IEEE, "IEEE standard procedures for measurement of power frequency electric and magnetic fields from AC power lines." IEEE, Piscataway, NJ, USA, pp. 1-40, Nov. 07, 2019, doi: 10.1109/IEEESTD.2020.9068517.
- H. F. CARLAK, Ş. ÖZEN, and S. BİLGİN, "Low-frequency exposure analysis using electric and magnetic field measurements and predictions in the proximity of power transmission lines in urban areas," Turkish Journal of Electrical Engineering and Computer Sciences, vol. 25, pp. 3994-4005, 2017, doi: 10.3906/elk-1608-312.
- [10] J. C. Salari, A. Mpalantinos, and J. I. Silva, "Comparative analysis of 2- and 3-D methods for computing electric and magnetic fields generated by overhead transmission lines," IEEE Transactions on Power Delivery, vol. 24, no. 1, pp. 338-344, Jan. 2009, doi: 10.1109/TPWRD.2008.923409.
- [11] T. Meriouma, S. A. Bessedik, and R. Djekidel, "Modelling of electric and magnetic field induction under overhead power line using improved simulation techniques," European Journal of Electrical Engineering, vol. 23, no. 4, pp. 289-300, Aug. 2021, doi: 10.18280/eiee.230402.
- M. L. P. Filho et al., "Upgrading urban high voltage transmission line: impact on electric and magnetic fields in the environment," in 2004 IEEE/PES Transmision and Distribution Conference and Exposition: Latin America (IEEE Cat. No. 04EX956), pp. 788– 793, doi: 10.1109/TDC.2004.1432482.
- [13] P. Gajšek, P. Ravazzani, J. Grellier, T. Samaras, J. Bakos, and G. Thuróczy, "Review of studies concerning electromagnetic field (EMF) exposure assessment in Europe: low Frequency fields (50 Hz–100 kHz)," *International Journal of Environmental* Research and Public Health, vol. 13, no. 9, p. 875, Sep. 2016, doi: 10.3390/ijerph13090875.
- [14] K. J. Fernie and S. J. Reynolds, "The effects of electromagnetic fields from power lines on avian reproductive biology and physiology: a review," Journal of Toxicology and Environmental Health, Part B, vol. 8, no. 2, pp. 127–140, Feb. 2005, doi: 10.1080/10937400590909022.
- L. Hardell and C. Sage, "Biological effects from electromagnetic field exposure and public exposure standards," Biomedicine & Pharmacotherapy, vol. 62, no. 2, pp. 104-109, Feb. 2008, doi: 10.1016/j.biopha.2007.12.004.
- [16] M. S. Markov, "Effects of electromagnetic fields on biological systems," Electromagnetic Biology and Medicine, vol. 32, no. 2,
- pp. 121–122, Jun. 2013, doi: 10.3109/15368378.2013.776333. I. Duhaini, "The effects of electromagnetic fields on human health," *Physica Medica*, vol. 32, p. 213, Sep. 2016, doi: 10.1016/j.ejmp.2016.07.720.
- International Commission on Non-Ionizing Radiation Protection, "Guide-lines for limiting exposure to time-varying electric and magnetic fields for low frequencies (1 Hz-100 kHz)," Health Physics, vol. 99, no. 6, pp. 818-836, Dec. 2010, doi: 10.1097/HP.0b013e3181f06c86.
- Ministry of Health, "Electric and magnetic fields and your health: information on electric and magnetic fields associated with transmission lines, distribution lines and electrical equipment." Ministry of Health, Wellington, New Zealand, 2013.
- R. Stam, "Comparison of international policies on electromagnetic fields: (power frequency and radiofrequency fields)," 2018.
- N. Y. Jayalakshmi and S. N. Deepa, "Modelling of electric and magnetic fields under high voltage AC transmission line," IOSR Journal of Electrical and Electronics Engineering, vol. 11, no. 3, pp. 24-31, 2016.
- S. Ghnimi, A. Rajhi, A. Gharsallah, and Y. Bizid, "Theoretical and experimental analysis of extremely low frequency magnetic field in the vicinity of the transformer station of overhead power lines," Journal of Electrical Engineering & Technology, vol. 13, no. 4, pp. 1655–1662, 2018.
- I. N. Ztoupis, I. F. Gonos, and I. A. Stathopulos, "Calculation of power frequency fields from high voltage overhead lines in residential areas," in 18th International Symposium on High Voltage Engineering, 2013, pp. 61-66.
- A. Z. El Dein, "Magnetic-field calculation under EHV transmission lines for more realistic cases," IEEE Transactions on Power Delivery, vol. 24, no. 4, pp. 2214–2222, Oct. 2009, doi: 10.1109/TPWRD.2009.2028794.
- [25] E. Salinas et al., "Mitigation techniques of power frequency magnetic fields originated from electric power systems," Electra, vol. 242, pp. 75–83, 2009.
- A. Canova, L. Giaccone, and V. Cirimele, "Active and passive shield for aerial power lines," in 25th International Conference on Electricity Distribution Madrid, 2019, no. 1096, pp. 1-5.
- [27] R. M. Radwan, M. Abdel-Salam, M. M. Samy, and A. M. Mahdy, "Passive and active shielding of magnetic fields underneath overhead transmission lines theory versus experiment," in Proceedings of the 17th International Middle East Power Systems
- Conference. Mansoura, 2015, pp. 1–10.
  P. Cruz Romero et al., "Magnetic field mitigation in power lines with passive and active loops," CIGRE, 2002.
- A. Z. El Dein, O. E. Gouda, M. Lehtonen, and M. M. F. Darwish, "Mitigation of the electric and magnetic fields of 500-kV overhead transmission lines," *IEEE Access*, vol. 10, pp. 33900–33908, 2022, doi: 10.1109/ACCESS.2022.3161932. S. Mirjalili, S. M. Mirjalili, and A. Lewis, "Grey wolf optimizer," *Advances in Engineering Software*, vol. 69, pp. 46–61, Mar.
- 2014, doi: 10.1016/j.advengsoft.2013.12.007.
- D. Rabah, B. Bentouati, R. A. El-Sehiemy, M. S. Shahriar, and H. R. E. H. Bouchekara, "Analysis of the optimized compensating loops effect on the magnetic induction due to very-high-voltage underground cable using grey wolf optimizer," Arabian Journal for Science and Engineering, vol. 48, no. 11, pp. 14407-14422, Nov. 2023, doi: 10.1007/s13369-023-07656-5.
- D. Reichelt, R. Scherer, R. Braunlich, and T. Aschwanden, "Magnetic field reduction measures for transmission lines considering power flow conditions," in Proceedings of 1996 Transmission and Distribution Conference and Exposition, 1996, pp. 486-492, doi: 10.1109/TDC.1996.547560.
- M. M. Saied, "Assessment and optimal passive-loop mitigation of power lines' magnetic fields," in 2008 Asia-Pacific Symposium on Electromagnetic Compatibility and 19th International Zurich Symposium on Electromagnetic Compatibility, May 2008, pp. 807-810, doi: 10.1109/APEMC.2008.4559998.
- [34] E. C. Caparelli and D. Tomasi, "An analytical calculation of the magnetic field using the biot savart law," Revista Brasileira de Ensino de Física, vol. 23, no. 3, pp. 284-288, Sep. 2001, doi: 10.1590/S1806-11172001000300005.
- R. Lings, "Overview of transmission lines above 700 kV," in Proceedings of the Inaugural IEEE PES 2005 Conference and Exposition in Africa, 2005, pp. 33-43, doi: 10.1109/PESAFR.2005.1611782.
- A. Mujezinovic, E. Turajlic, A. Alihodzic, N. Dautbasic, and M. M. Dedovic, "Novel method for magnetic flux density estimation in the vicinity of multi-circuit overhead transmission lines," IEEE Access, vol. 10, pp. 18169-18181, 2022, doi: 10.1109/ACCESS.2022.3149393.
- R. Deltuva and R. Lukočius, "Distribution of magnetic field in 400 kV double-circuit transmission lines," Applied Sciences, vol.

- 10, no. 9, p. 3266, May 2020, doi: 10.3390/app10093266.
- [38] K. Yamazaki, T. Kawamoto, and H. Fujinami, "Requirements for power line magnetic field mitigation using a passive loop conductor," *IEEE Transactions on Power Delivery*, vol. 15, no. 2, pp. 646–651, Apr. 2000, doi: 10.1109/61.852999.
- [39] A. R. Memari and W. Janischewskyj, "Mitigation of magnetic field near power lines," *IEEE Transactions on Power Delivery*, vol. 11, no. 3, pp. 1577–1586, Jul. 1996, doi: 10.1109/61.517519.
- [40] R. Mardiana and M. Poshtan, "Mitigation of magnetic fields near transmission lines using a passive loop conductor," in 2011 IEEE GCC Conference and Exhibition (GCC), Feb. 2011, pp. 665–668, doi: 10.1109/IEEEGCC.2011.5752635.
- [41] W. T. Kaune and L. Zaffanella, "Analysis of magnetic fields produced far from electrical power lines," in Proceedings of the 1991 IEEE Power Engineering Society Transmission and Distribution Conference, 1992, pp. 735–742, doi: 10.1109/TDC.1991.169587.
- [42] N. I. of Environmental Health Sciences, N. I. of Health, and Others, "Electric and magnetic fields associated with the use of electric power," National Institute of Environmental Health Sciences National Institutes of Health, 2002.
- [43] A. Canova, F. Fabio, L. Giaccone, A. Guerrisi, and M. Repetto, "Magnetic field mitigation by means of passive loop: technical optimization," *COMPEL The international journal for computation and mathematics in electrical and electronic engineering*, vol. 31, no. 3, pp. 870–880, May 2012, doi: 10.1108/03321641211209762.
- [44] P. Cruz, C. Izquierdo, and M. Burgos, "Optimum passive shields for mitigation of power lines magnetic field," IEEE Transactions on Power Delivery, vol. 18, no. 4, pp. 1357–1362, Oct. 2003, doi: 10.1109/TPWRD.2003.817754.
- [45] J. C. Bravo-Rodríguez, J. C. Del-Pino-López, and P. Cruz-Romero, "A Survey on optimization techniques applied to magnetic field mitigation in power systems," *Energies*, vol. 12, no. 7, p. 1332, Apr. 2019, doi: 10.3390/en12071332.
- [46] M. Ksi\każkiewicz, "Passive loop coordinates optimization for mitigation of magnetic field value in the proximity of a power line," Computer Applications in Electrical Engineering, vol. 13, pp. 77–87, 2015.
- [47] M. Rebolini, M. Forteleoni, and D. Capra, "Passive cancellation loops: case study, model simulation and field test on a real HV overhead line in Italy: electromagnetic computation and optimization," in 2017 AEIT International Annual Conference, Sep. 2017, pp. 1–6, doi: 10.23919/AEIT.2017.8240502.
- [48] P. Cruz, J. M. Riquelme, A. de la Villa, and J. L. Martínez, "Ga-based passive loop optimization for magnetic field mitigation of transmission lines," *Neurocomputing*, vol. 70, no. 16–18, pp. 2679–2686, Oct. 2007, doi: 10.1016/j.neucom.2006.05.016.
- [49] P. C. Romero, J. R. Santos, J. C. del Pino Lopez, A. de la Villa Jaen, and J. L. M. Ramos, "A comparative analysis of passive loop-based magnetic field mitigation of overhead lines," *IEEE Transactions on Power Delivery*, vol. 22, no. 3, pp. 1773–1781, Jul. 2007, doi: 10.1109/TPWRD.2007.899784.
- [50] K. Budnik and W. Machczyński, "Reduction of magnetic field from a power line using a passive loop conductor," Computer Applications in Electrical Engineering, vol. 11, pp. 46–63, 2013.
- [51] J. A. Brandao Faria and M. E. Almeida, "Accurate calculation of magnetic-field intensity due to overhead power lines with or without mitigation loops with or without capacitor compensation," *IEEE Transactions on Power Delivery*, vol. 22, no. 2, pp. 951– 959, Apr. 2007, doi: 10.1109/TPWRD.2006.883025.
- [52] S. Celozzi, "Active compensation and partial shields for the power-frequency magnetic field reduction," in *IEEE International Symposium on Electromagnetic Compatibility*, 2002, vol. 1, pp. 222–226, doi: 10.1109/ISEMC.2002.1032478.
- [53] C. Buccella, M. Feliziani, and V. Fuina, "ELF magnetic field mitigation by active shielding," in *Industrial Electronics*, 2002. ISIE 2002. Proceedings of the 2002 IEEE International Symposium on, 2002, pp. 994–998, doi: 10.1109/ISIE.2002.1025869.
- [54] S. Barsali, R. Giglioli, and D. Poli, "Active shielding of overhead line magnetic field: design and applications," *Electric Power Systems Research*, vol. 110, pp. 55–63, May 2014, doi: 10.1016/j.epsr.2014.01.005.
- [55] M. Ziolkowski and S. Gratkowski, "Active, passive and dynamic shielding of static and low frequency magnetic fields," in VXV International Symposium on Theoretical Engineering, 2009, pp. 1–5.
- [56] P. C. Romero, C. I. Mitchell, and M. B. Payan, "Optimal design of active shielding for power lines," in 14th Power Systems Computation Conference, 2002, pp. 24–28.
- [57] R. Falsaperla, G. Spagnoli, and P. Rossi, "Electromagnetic fields: principles of exposure mitigation," *International Journal of Occupational Safety and Ergonomics*, vol. 12, no. 2, pp. 195–200, Jan. 2006, doi: 10.1080/10803548.2006.11076683.
- [58] Z. Mustaffa, M. H. Sulaiman, and M. N. M. Kahar, "LS-SVM hyper-parameters optimization based on GWO algorithm for time series forecasting," in 2015 4th International Conference on Software Engineering and Computer Systems (ICSECS), Aug. 2015, pp. 183–188, doi: 10.1109/ICSECS.2015.7333107.
- [59] O. M. A. Ahmed and H. Kahramanli, "Meta-heuristic solution approaches for traveling salesperson problem," *International Journal of Applied Mathematics Electronics and Computers*, vol. 6, no. 3, pp. 21–26, 2018.
- [60] R. Saravanan, S. Subramanian, V. Dharmalingam, and S. Ganesan, "Generation scheduling of wind thermal integrated power system using grey wolf optimization," *J. Electr. Electron. Eng.*, vol. 11, no. 6, pp. 48–55, 2016.
- [61] Z. Li, Y. He, H. Li, Y. Li, and X. Guo, "A Novel discrete grey wolf optimizer for solving the bounded knapsack problem," in International Symposium on Intelligence Computation and Applications, 2019, pp. 101–114, doi: 10.1007/978-981-13-6473-0\_10.
- [62] S. U. Khan, M. K. A. Rahim, and L. Ali, "Correction of array failure using grey wolf optimizer hybridized with an interior point algorithm," Frontiers of Information Technology & Electronic Engineering, vol. 19, no. 9, pp. 1191–1202, Sep. 2018, doi: 10.1631/FITEE.1601694.
- [63] W. Lei, W. Jiawei, and M. Zezhou, "Enhancing grey wolf optimizer with levy flight for engineering applications," *IEEE Access*, vol. 11, pp. 74865–74897, 2023, doi: 10.1109/ACCESS.2023.3295242.
- [64] R. B. Thanoon and B. A. Mitras, "Modified grey wolf optimization algorithm by using classical optimization methods," International Journal of Computer Networks and Communications Security, vol. 7, no. 3, pp. 49–60, 2019.
- [65] R. Djekidel, S. A. Bessedik, P. Spiteri, and D. Mahi, "Passive mitigation for magnetic coupling between HV power line and aerial pipeline using PSO algorithms optimization," *Electric Power Systems Research*, vol. 165, pp. 18–26, Dec. 2018, doi: 10.1016/j.epsr.2018.08.014.
- [66] M. Milutinov, A. Juhas, and M. Prša, "Electromagnetic field underneath overhead high voltage power line," in 4th International Conference on Engineering Technologies ICET, 2009, pp. 1–5.
- [67] Z. Liang, X. Li, X. Gu, and Y. Jiang, "Elliptically polarized magnetic field of electric power lines and mitigation by passive shielding," in 2015 7th Asia-Pacific Conference on Environmental Electromagnetics (CEEM), Nov. 2015, pp. 53–56, doi: 10.1109/CEEM.2015.7368626.
- [68] J. Hardy and E. Boje, "Distribution pole monitoring using magnetic field characterization," SAIEE Africa Research Journal, vol. 110, no. 3, pp. 145–152, Sep. 2019, doi: 10.23919/SAIEE.2019.8732786.
- [69] M. Misakian, "ELF electric and magnetic field measurement methods," in 1993 International Symposium on Electromagnetic Compatibility, 1993, pp. 150–155, doi: 10.1109/ISEMC.1993.473761.

- [70] CIGRE, "Characterisation of ELF magnetic fields." e-cigre.org, 2007.
- [71] Y. Xie, S. Li, C. Wang, and D. Yang, "Analysis and treatment of current unbalance abnormal situation of 750 kV double-circuit parallel transmission line," *International Journal of Metrology and Quality Engineering*, vol. 14, no. 2, Apr. 2023, doi: 10.1051/ijmqe/2023001.

#### **BIOGRAPHIES OF AUTHORS**



Salah-Eddine Houicher was sorn in Laghouat, Algeria, on November 11, 1992. He graduated from Ammar Telidji University of Laghouat, Algeria, faculty of technology, in 2012. He received the master degrees in electromagnetic compatibility of industrial systems in 2017, from Laghouat University-Algeria. He is PhD student at the University of Amar Telidji in Laghouat, department of electrical engineering. faculty of technology, Algeria. His research interest concern: electromagnetic fields, high voltage electrical engineering, numerical simulation, electromagnetic compatibility and optimization techniques. Correspondence address: Department of electrical engineering, faculty of technology, University Amar Telidji in Laghouat -Algeria. He can be contacted at email: s.houicher@lagh-univ.dz.



Rabah Djekidel was born in Laghouat, Algeria, on March 25, 1968. He graduated the University of ENSET Technique in Laghouat, Algeria, in 1991. He received the magister and Ph.D. degrees in electrical engineering, respectively in 2010, 2015 from USTO Oran University and Laghouat University, Algeria. He is professor at the department of electrical engineering, faculty of technology; University of Amar Telidji in Laghouat, Algeria. His research interest concern: electromagnetic interference (EMI) fields, high voltage engineering, numerical modeling and simulation, optimization techniques. Correspondence address: department of electrical engineering, faculty of technology, University Amar Telidji in Laghouat -Algeria. He can be contacted at email r.djekidel@lagh-univ.dz.

